crystals

MDPI

Article

Revisiting Alloy Design of Al-Base Alloys for Potential Orthotics and Prosthetics Applications

Muhammad Farzik Ijaz * and Faraz Hussain Hashmi

Mechanical Engineering Department, College of Engineering, King Saud University, P.O. Box 800, Riyadh 11421, Saudi Arabia

* Correspondence: mijaz@ksu.edu.sa

Abstract: The primary objective of this research was to open a promising avenue for designing new low-cost precipitation-hardened Al base alloys in semblance with the desired mechanical properties that can be exploited in the fabrication of lightweight exoskeleton frames, prosthetics, and wheelchair components. In multicomponent Al-Cu-based systems (2xxx), the substitution of elements such as copper (Cu), magnesium (Mg), and akin Cu/Mg ratio are mainly manipulated to improve the mechanical strength of these alloys. Nonetheless, these kinds of alloying optimizations are not well suited from the cost and sustainability points of view. The starting point of the present work is to screen out the optimum value of the Ag/Sn ratio, which can be a potential substitute for the conventional Cu/Mg alloy ratio in Al-Cu-Mg-based ternary alloys without sacrificing its key features of mechanical properties. Based on our microstructural and mechanical results, it was found that the chemical composition and microstructure were the most important variables influencing the mechanical properties. The increase in the mechanical strength of our alloys was mainly attributed to the precipitation hardening phenomenon. Typically, at peak-aged conditions, the correlation between the mechanical and subsequent microstructural analysis revealed that the synergistic increase in Ag and Sn content in the Al-Cu-Mg-based alloy led to an improvement in the mechanical strength and its trade-offs by changing the shape and distribution of the micron-scaled second phase in the matrix. From optical microscopy and subsequent scanning electron microscopy analyses, this continuous precipitated phase in the matrix is identified as the Mg_2Sn phase, which is mainly elicited from the solid-state reaction during artificial aging treatment. Indeed, the presence of suitable microstructure at the peak aged condition that has uniformly dispersed, micron-scale Mg_2Sn phase proved to be very useful in blocking the dislocation glide and increasing the mechanical strength of the alloys during tensile testing. This combination of precipitation-hardening phases has not been previously observed in alloys with higher or lower Cu/Mg ratios. Among the studied alloys, the alloy having Ag/Sn ratio of 23 (and chemical composition of Al-4 Cu-0.5 Mg-0.7 Ag-0.03 Sn (wt.%)-T6 (denoted as Al-loy-4) exhibited an average ultimate tensile strength of 450 MPa which is almost four times larger than the pure aluminum having an ultimate tensile strength of 90 MPa currently used in healthcare and medical industries.

Keywords: lightweight components; aluminum; composition; Ag/Sn ratio; peak aged condition; mechanical properties

check for updates

Citation: Ijaz, M.F.; Hashmi, F.H. Revisiting Alloy Design of Al-Base Alloys for Potential Orthotics and Prosthetics Applications. *Crystals* **2022**, *12*, 1699. https://doi.org/10.3390/cryst12121699

Academic Editor: Shouxun Ji

Received: 21 October 2022
Accepted: 20 November 2022
Published: 23 November 2022

Publisher's Note: MDPI stays neutral with regard to jurisdictional claims in published maps and institutional affiliations.

Copyright: © 2022 by the authors. Licensee MDPI, Basel, Switzerland. This article is an open access article distributed under the terms and conditions of the Creative Commons Attribution (CC BY) license (https://creativecommons.org/licenses/by/4.0/).

1. Introduction

In rehabilitative fields, the devices such as Prostheses (artificial legs and hands), orthoses (braces and splints), and/or healthcare instruments such as metal-framed transport wheelchairs are widely used to enable people with physical impairments or functional limitations to live healthy social life [1–3]. Prevalently, from the viewpoint of potential functional outcomes in the medical field, it is critical to substitute traditional heavy metal components of Iron (Fe) with some lightweight metal components [4,5]. For example, Aluminum (Al) components can substantially reduce the weight of many exoskeleton

devices and will be far easier to propel when compared to their heavier counterparts [6,7]. Consequently, in the recent past, owing to the intrinsic property of being lightweight, aluminum and its alloys have garnered considerable potential in the medical industry, from laboratory-designed materials to advanced structural materials. Owing to the fact that the weight of Al alloys is one-third of the commercially available steel components, which makes it promisingly versatile for several applications, including wheelchairs, where less energy expenditure by the patient during service and cost are prevalent [8,9]. Unfortunately, the strength of Aluminum alloys is only half of that of commercial steel. The two common aluminum alloys used in the medical field are 7005 T-6 and 6061T-6 alloys; they have an ultimate tensile strength of 350 MPa and 310 MPa, respectively [8–10]. Hence for durability, the improvement in the mechanical properties, especially the strength-to-weight ratio of Al alloys, still remains a significant concern that needs to be resolved.

It is noteworthy to mention here that the most researched age-hardenable aluminum alloy in the past was the 2xxx series alloy, also known as the Al-Cu-(Mg) system. The development of many 2xxx series alloys was initiated as a result of early efforts to lighten auto body panels which are made from steel. The 2014 and 2024 high-strength alloys, on which these automobile 2xxx alloys were based, had their copper content drastically lowered to fulfill formability requirements while still keeping enough mechanical strength to meet steel's dent resistance performance. The 2xxx series alloys are often more durable when aged and solutionized as compared to the 6xxx system (due to increased solid solution and precipitate fractions, respectively) [11,12]. Hence, owing to the very low cost per unit weight, they have stupendous potential to have emerged as a promising structural material in the fabrication of exoskeleton frames, prosthetics, and wheelchair components.

To date, the Al-Cu-based alloys commonly designated as the AA2xxx series are increasingly being studied over the years because copper has a significant in improving the mechanical properties of wrought Al-based alloys. Nonetheless, in any kind of Al-Cu-based alloy weather, it is in an as-cast or wrought state and responds to heat treatment, and its mechanical properties are influenced accordingly by the solution treatment and aging treatment condition as well. However, in most cases, the mechanical strengthening effect is more evident when Cu content is fixed below 6 wt.% [13,14]. Indeed, with copper as a major alloying element in the AA2xxx series and with heat treatment processes such as the age hardening or precipitation hardening methods, the hardness of the aluminum matrix could be significantly enhanced by the formation of Al_2Cu precipitates [15]. From a view of ternary Al-Cu-Mg alloy, Liu et al. reported the mechanical properties of ternary Al-Cu-Mg alloy and reported the yield strength (YS) of 395 MPa and ultimate tensile strength (UTS) of 446 MPa. Interestingly, the mechanical properties of ternary Al-Cu-Mg were increased by the addition of 0.3 (wt.%) Si such that the quarternary Al–5.0Cu–0.3Mg–0.3Si (wt.%) alloy exhibited superior yield strength of 424 MPa and ultimate tensile strength of 466 MPa. They claimed that the improvement in mechanical properties was attributed to Si-containing Q" precipitates pre-formed in the initial aging stage by virtue of Q"-type precipitates [16].

Likewise, the addition of Mg as a ternary element in Al-Cu-based alloys has the capability of further enhancing the strengths of this kind of alloy by virtue of adjustment in Cu/Mg ratio and resulting S-phase (Al_2CuMg) precipitates during the aging process [17]. From the viewpoint of mechanical strength, another important criterion is the addition of ternary or quaternary micro-alloying in Al-Cu-based alloys. Several studies have been performed to examine the precipitation process and its consequent on mechanical characteristics by the influence of a small amount of alloying addition in binary Al-Cu alloys [18–29].

In the same fashion, the improvement in the precipitation aging responses was also enhanced by the introduction of Ag addition in Al-Cu-Mg alloys [30]. It is because adding Ag to Al-Cu-Mg alloys encourages the formation of Mg-Ag co-clusters which serve as an initial precursor for the nucleation of highly desirable well-known Ω- phase precipitates. This Ω phase exhibits an excellent combination of great strengthening ability and high thermal stability, making Al-Cu-Mg-Ag alloy an ideal candidate for aerospace applications at elevated temperatures. However, the optimum value of Ag in Al-Cu-Mg based shall

be chosen to facilitate the formation of Ω- phase in Al-Cu-Mg alloys. It is because, in the previous literature, it is also claimed that the addition of Ag from 0.4–0.8% failed to enhance the Ω- phase precipitation formation [31]. Hence for the reason of having a positive outcome, the amount of quaternary element Silver (Ag) must be restricted between 0.3–0.6 wt.% [32–34].

Similarly, in this context, it has also been reported that the addition of Tin (Sn) in bi-nary Al-Cu alloys increases the hardness values, which is attributed to the refinement and homogeneous dispersion of the strength-providing θ′ precipitate phase (Al_2Cu) [35,36]. At the same time, it was also reported that the addition of Sn content in Al-1.7 at. % Cu up to 0.01 at. % Sn dramatically shortens the time to reach peak hardness and increases peak hardness value [37–43]. For example, Banerjee et al. [44] added 0 to 0.1 wt.% of Sn in the as-cast Al-6.2% Cu-0.6% Mg alloy system. It was shown that the overall grain size was reduced when Sn was added beyond 0.06 wt.%., which ultimately resulted in the improvement of mechanical properties such as the ultimate tensile strength of Al-Cu-Mg-based alloy [45,46].

Quite recently, the addition of Ag and Sn has been taken synergistically to evaluate their advantageous effect on the precipitation kinetics and resulting mechanical properties. For instance, it has been demonstrated that the precipitation process in Al-Cu-Mg-Sn and Al-Cu-Mg-Ag-Sn alloys can be tuned for a suitable outcome [47,48]. From previous literature, it was claimed that Sn, when added simultaneously with Ag in Al-Cu-Mg-based alloys, has positive research significance [47]. For example, it was demonstrated experimentally that the trace amount of Sn, on the one hand, increases the hardness throughout the aging process when it is added in combination with Ag; it further increases the hardness and shortens the time to reach peak hardness. The increase in hardness via Sn is mainly attributed due to the homogenous distribution of the S phase. Sn element can also induce an excellent impact on the alloys by forming Mg_2Sn precipitate. These precipitates, when distributed at sub-grain boundaries, inhibit the recrystallized grain growth during the solution treatment. Furthermore, Sn has dramatically stronger binding energy with vacancy, so it is beneficial in suppressing the natural aging process and also refines the precipitate by trapping the vacancies [48,49]. Collectively, all of these aforementioned studies are very helpful for understanding and utilizing the appropriate alloying design route for increasing the mechanical strength and its trade-offs together in the Al-Cu-Mg alloy system. Despite this fact, experimental results displaying the synergistic approach, i.e., the addition of Sn and Ag content and adjustment in Ag/Sn for acquiring optimized experimental results in terms of mechanical properties, have scarcely been presented in literature so far. Primarily, the main objective of the current study revisits and discusses the new design strategy based on the addition of two quaternary and quinary elements in a conventional Al-Cu-Mg alloying system in semblance with the desired mechanical properties.

From the viewpoint of alloy design, the selection of fixed content of the principal alloying elements, i.e., Cu and Mg, are chosen on the basis thermodynamic binary phase diagram carefully; actually, the concentrations of Mg and Cu were chosen in a way that chemical composition falls in the (α + θ + S) and (Ω) phase fields region at approximately 190 °C, respectively [19,20]. However, more importantly, in our alloy design strategy, the content of qua-ternary-element Ag and quinary element Sn were strictly varied between two levels to seek optimum balance in terms of chemical composition. Explicitly, the corresponding elemental content for Ag and Sn in our designed Al-Cu-Mg-xAg-ySn alloying system were as per the following sequence x = 0.3 and 0.6 wt.% and y = 0.01, 0.03, respectively. At the same time, the amount of quinary element Sn in this alloying system was chosen between 0.01 and 0.03 wt.%. This compositional design was basically aimed to explore the optimal value of the Ag/Sn ratio advantageous in accomplishing the optimal strengthening features such as solid solution strengthening and precipitation hardening. Consequently, on the other hand, a detailed investigation was performed to characterize the microstructural evolution of Al-Cu-Mg ternary alloy with different Ag/Sn ratios. From experimental results, it is found out that the Al-4 Cu-0.5 Mg-0.7 Ag-0.03 Sn-T6 (denoted as Alloy-4) exhibited excellent balance in the mechanical characteristics having the mechanical

ultimate tensile strength of almost 450 MPa, which is superior to the commercially available 7005 T-6 aluminum (350 MPa) and 6061 T-6 aluminum (310 MPa) used in the medical field [4,7–10]. The formation of diffusion-controlled Mg_2Sn precipitates was plausible to ascribe to the improvement of the mechanical properties. In summary, our present work provides new knowledge for the quantitative strength optimization of Al-based alloys for tailoring potential applications in the medical field. We show that the designed alloy with high Sn and intermediate Ag/Sn ratio has better mechanical properties due to the coexistence of immobile crystalline defects such as Mg2Sn and θ type precipitates. Interestingly, the peak hardness values and the ultimate tensile are much greater than the alloys in which the Cu/Mg ratio was manipulated to achieve the target of high strength in Al-based alloys. Thus, with the presence of intriguing properties combined with the low-cost design, our newly developed can create a new frontier of prominence from laboratory-designed materials to advanced structural materials orthotics and prosthetics applications, mainly in prosthetic pylons, orthotic up-rights, wheelchairs, and upper extremity devices.

2. Materials and Methods

To investigate the effect of Ag/Sn ratio contents in Al-4Cu-0.5Mg-*x*Ag-*y*Sn alloy (where x = 0.3 and 0.6 wt.% and y = 0.01 and 0.03, respectively). In this context, four compositions with two different levels of Ag/Sn ratio were designed. In the preparation of the four ingots, the raw materials (Al, Cu, Mg, Ag, and Sn) were melted in the induction furnace at 730 °C and then poured into a steel mold with a dimension of 100 mm (length) × 60 mm (width) × 16 mm (thickness). The samples were cooled at room temperature. After removing the samples from the mold, each sample was homogenized in an air furnace at 540 °C for 24 h, followed by furnace cooling. This homogenization is necessary to make sure that the composite elements have a full and uniform distribution of alloying elements. The chemical compositions of each ingot were checked using a metal analyzer (Spectromax machine) to confirm the individual percentage of respective alloying addition in the prepared alloy, respectively. Table 1 summarizes the nominal composition of the four prepared alloys with their designed Ag/Sn ratio investigated in the present study with their assigned nomenclatures. The nominal composition was Al-4 Cu-0.5 Mg-0.4 Ag-0.01 Sn (wt.%) (hereafter referred to as Alloy-1: Ag/Sn = 32), Al-4 Cu-0.5 Mg-0.7 Ag-0.01 Sn (wt.%) (hereafter referred to as Alloy-2: Ag/Sn = 63), Al-4 Cu-0.5 Mg-0.4 Ag-0.03 Sn (wt.%) (hereinafter referred to as Alloy-3 Ag/Sn = 13) and Al-4 Cu-0.5 Mg-0.7 Ag-0.03 Sn (wt.%) (hereafter referred to as Alloy-4: Ag/Sn = 23). After the homogenization process, the prepared four ingots were put through the mechanical hot rolling operation. Before the hot rolling treatment, the ingot with dimensions 15 × 40 × 100 mm was inserted inside the furnace of hot roll and heated to 450 °C for 2 h. Then, the ingot was removed from the furnace and directly hot rolled from 15 mm to approximately 2.5 mm (~84% reduction in thickness). The reduction of thickness was performed in multiple passes with a 0.4 mm reduction at each pass and an average speed of 1.75 m/min. The hot rolling steps were performed on the as-cast ingot, mainly to mitigate the vacancies, pores, and casting-related defects. It was expected that some defects, such as gas porosity, existed in the samples after die-casting. Thus, in roughly 18 passes, the samples were hot rolled from 15 mm to 2.5 mm (a thickness reduction of 84%). The Alloy-1, Alloy-2, Alloy-3, and Alloy-4 specimens underwent solid solution treatment (SST) at 520 °C for 8 h after the homogenization procedures and were subsequently water quenched to achieve the supersaturated solution of the phase at room temperature. After solution treatment, the artificial aging procedure was carried out on each specimen. Firstly, the preparation of the solute bath was performed by mixing 50% of Sodium Nitrate and 50% of Potassium Nitrate. The mixture was kept inside the furnace at 190 °C until it became fully liquid for around 3 h. Secondly, the preparation of the sample alloys was performed by cutting the sheet into small pieces of 20 × 20 mm.

Table 1. Results of the chemical composition and Ag/Sn ratio of the experimental alloys.

Alloys: Nomenclature	Ag/Sn Ratio	Chemical Composition (wt.%)				
		Cu	Mg	Ag	Sn	Al
Alloy-1	32	4	0.50	0.30	0.01	Balance
Alloy-2	63	4	0.50	0.70	0.01	Balance
Alloy-3	13	4	0.50	0.30	0.03	Balance
Alloy-4	23	4	0.50	0.70	0.03	Balance

To elucidate the influence of composition on age-hardening behavior, specifically hardness testing was carried out following the artificial aging treatment method, which is undertaken mainly to assess the peak hardening condition. Nondestructive hardness testing as a function of aging time can provide a hardness vs. aging graph that can predict the time required to reach maximum strength under the isothermal aging scenarios. In our particular case, hardness testing was performed to determine the peak aged hardening value concerning the compositional design; that is, the adjustment in Ag/Sn ratio in ternary Al-Cu-Mg alloy. The microhardness measurement is a well-known nondestructive technique that is widely used to evaluate the age-hardening response of the alloy both at the solution treated and after the artificial aging process. In the present study, the hardness measurement was undertaken while using Vickers hardness testing equipment (WOLPERT UH930, Wilson Hardness, Shanghai, China); eight indents were used to compute the average Vickers hardness number (VHN) of each specimen of Alloy-1, Alloy-2, Alloy-3, and Alloy4 that had been aged for a variable amount of time (WOLPERT UH930, Wilson Hardness, Shanghai, China). Each indentation was made by applying a 10 kg load for 15 s.

Then, tensile testing was performed at room temperature (RT; 25 °C) to determine how the compositional design (i.e., Ag/Sn ratio) affected the mechanical properties. Each set of the peak aged specimen from four alloys, i.e., Alloy-1, Alloy-2, Alloy-3, and Alloy-4, was subjected to uniaxial tension at room temperature. The well-known ASTM E-8 standard served as the guide for preparing the geometry of the tensile samples. The tensile testing on each specimen of Alloy-1, Alloy-2, Alloy-3, and Alloy4 was performed on a computer-controlled tensile testing apparatus (Instron, University Ave, Norwood, MA, USA). During the tensile testing, the parameter of strain rate was fixed at 10^{-3} s^{-1}. Measurements of total strain were ascertained by utilizing an extensometer (epsilon 35420125M). The typical engineering stress-strain curves of each specimen were also sketched from the load and extension data recorded during the tensile testing. To interpret the important mechanical properties from the tensile testing, such as the yield stress (σ_{YS}), ultimate tensile stress (σ_{UTS}), and percentage elongation (ductility) of the designed alloy specimens at peak-aged state conditions, were recorded, respectively. The repeatability of the measured data and average were examined using at least four sets of samples for each composition at peak-aged state conditions.

In order to observe the microstructural features, such as the average grain size, optical microscopy observation was made for each specimen. Similarly, micro-level image analysis using ImageJ functions also has been utilized to explore and determine small precipitate sizes. For optical observation, the mirror-like surface finish for all the specimens for each alloy was prepared by 0.05 μm alumina particle polishing; before polishing, the surface specimen was also grounded by 500 to 1200 grit emery papers. The specimens were etched following ASTM E 407-99 standard (2 mL HF, 3 mL HCl, 5 mL HNO_3, and 200 mL H_2O). Microstructural observation etching is vital to distinguish between grain boundaries as well as to make the various phases visible through variations in brightness, form, and color. An optical microscope instrument (Olympus BX51M, Tokyo, Japan) was used to investigate the optical microstructures after surface etching treatment.

Scanning electron microscopy (SEM) was performed using a JXA-840A electron probe microanalysis (JEOL, Tokyo, Japan); this analysis was carried out to accomplish two pur-

poses. Firstly, to analyze different particles and grain structures at higher resolution in the form of SEM images. Secondly, to have a quantitative analysis of the composition by utilizing the EDS analysis. The same samples of optical microscopy, which were mounted on the resin, were used. The sample for the SEM observations needs to be electrically connected to the sample holder to prevent the electron beam from "charging" the sample and distorting the image. This is usually performed through conductive tape. However, not only is the SEM used with the EDS and backscattered, but also it is used to clarify the content of the particles and/or precipitates.

Furthermore, the phase constitutions in the peak aged (PA) treatment were investigated while using an X-ray diffractometer (Model: D-8 Discover, Bruker, Berlin, Germany) with Cu K monochromatic X-ray radiation, tube current of 15 mA, and voltage of 30 kV; measurements were made at room temperature.

3. Results and Discussion

3.1. Age-Hardening Response of Al-Cu-Mg-Ag-Sn Alloys

In order to understand the age-hardening behavior of the presently studied alloy with respect to their compositional design, that is, the Ag/Sn ratio, microhardness testing was performed on Alloy-1, Alloy-2, Alloy-3, and Alloy-4 specimens. The curve revealing the age-hardening response is obtained after the completion of three heat treatment steps which includes solution treatment, quenching, and aging. Figure 1 shows the age-hardening curve of Alloy-1, Alloy-2, Alloy-3, and Alloy-4, respectively, after being aged artificially at 190 °C for varied periods. When comparing the results from the age hardening curve, it can be observed that among the four alloys, the hardness values of Alloy-4 in the solution-treated condition, which is for 0 h, is higher than Alloy-1, Alloy-2, and Alloy-3 specimens, respectively. This rise in hardness value may be attributed form the chemical composition impact, as Alloy-4 has a higher content of Ag and Sn elements. The solid solution hardening effect in Aluminum alloys is increased with the atomic size difference. It should be noted that the atomic sizes of Al, Ag, and Sn are known to be 0.143 nm, 0.144 nm, and 0.162 nm, respectively [50]. Thus as per the difference in atomic size, the quantitative solution hardening effect of Sn would be stronger than Ag in our alloying system. Thus, based on the aforementioned reason, it is reasonably conceivable that the higher hardness values, specifically in Alloy-4, are a result of localized lattice distortion from the solute content that subsequently generates a higher energy barrier against dislocation movement under the indentation and tweaks well-known solution-hardening phenomenon. A similar effect has also been observed in many metallic alloys [51,52].

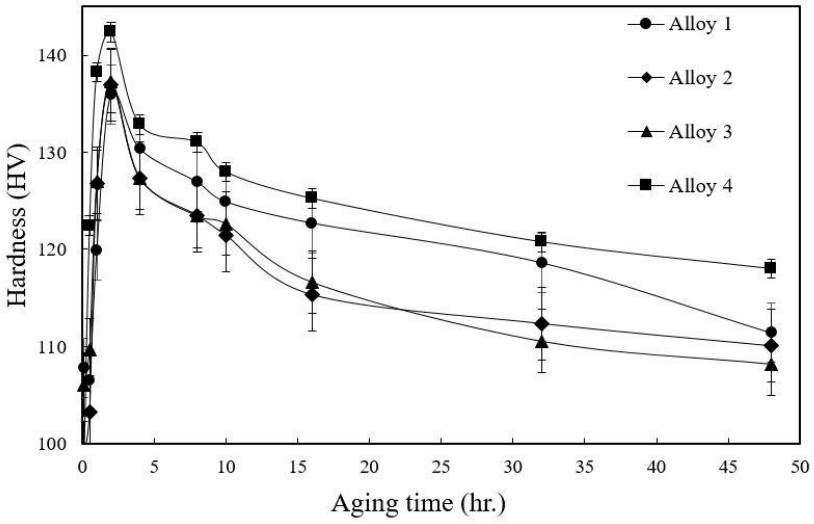

Figure 1. Evolution of microhardness of Alloy-1, Alloy-2, Alloy-3 and Alloy-4 specimens as a function of aging time.

Moving ahead, it is clear that all alloys exhibit a tendency to increase hardness values as the artificial aging process progresses, which is consistent with previously published research [14,17,18,47]. Nonetheless, the compositional design of the alloys, as well as the potential production of secondary precipitation phases from the supersaturated Al matrix, can be linked to the monotonic increase in hardness values shown in the case of our developed alloys. Ultimately the hardening propensity typically rises with aging time, reaching a maximum value (Peak aged state—PA), and then gradually declines with more aging, resulting in an overaged point (T7).

It can be observed that the hardness of all four alloys begins to decrease after a peak aging time of 2 h. Indeed, the peak aging time for Alloy-1, Alloy-2, Alloy-3, and Alloy-4 is almost the same, and it is attributed to be 2 h. However, the average value of hardness at the peak aging time was around 136 HV at 2 h for Alloy-1, 137 HV for Alloy-2, 138 Hv for Alloy-3, and about 142 Hv for Alloy-4. Thus this higher value of hardness at peak aging time for Alloy-4 could be inferred from the compositional effect, which is higher contents of Ag and Sn elements, and most importantly, the strengthening associated with grain boundary and precipitates could also not be neglected. The complex interactions of these defects are widely reported in the literature, revealing the influence of the dependence of age hardening behavior on precipitate geometry (e.g., shape, size) formed during age treatment [8,13,17,39,43,47,48,51,52]. For the same reason, a detailed study on the microstructure and phase analysis of each Alloy-1, Alloy-2, Alloy-3, and Alloy-4 specimens at peak aged condition were carried out, respectively, and will be discussed in the next sections.

3.2. Comparison of Room Temperature Mechanical Properties of Peak-Aged Alloys

Figure 2 shows the representative stress-strain curves of Alloy-1, Alloy-2, Alloy-3, and Alloy-4 specimens after the peak aged condition. Analysis of the tensile stress-strain curves from the present study allows us to determine the effect of compositional design on the room-temperature mechanical properties. As seen in Figure 2, typically, the ultimate tensile strength (σ_{UTS}) was strongly influenced by the compositional design as it gradually increased with increasing Ag and Sn contents. From Figure 2, the ultimate tensile strength (σ_{UTS}) for Alloy-1, Alloy-2, Alloy-3, and Alloy-4 specimens was recorded as 429 MPa, 435 MPa, 434 MPa, and 446. MPa, respectively. There was not a big statistical difference in the mechanical properties of each alloy, as the specimens were produced from the same initial ingot. Indeed, Alloy-4, containing a high concentration of Ag and Sn, led to positive synergistic effects in terms of mechanical properties. Among the alloys investigated in this study, the Alloy-4 displayed a balance in the mechanical properties, specifically showing the ultimate tensile strength (σ_{UTS}), yield strength (σ_{YS}), and percentage elongation (ε) are 446 MPa, 390 MPa, and 10% respectively. A comparison of the peak hardness value and Ultimate tensile strength values (σ_{UTS}) of the common purer Al and Al-base alloys, which are used in the medical field, is listed in Table 2. In addition, for the sake of comparison, the salient mechanical characteristics are also presented in the present study. Indeed, from comparison, the presently studied compositions revealed better mechanical properties. The improvement in our presently studied alloying system was very significant when compared to traditional lightweight Al-based alloys already applied in the medical field. For example, Al-4 Cu-0.5 Mg-0.7 Ag-0.03 Sn (wt.%)-T6 (denoted as Alloy-4) exhibited improvement in ultimate tensile strength of more than 300% when compared to pure Al [8], 44% when compared to 6061 T-6 aluminum [9] and 28 % when compared to 7005 T-6 aluminum [10]. From evidence from the past literature, it is convincing that the increase in tensile strength after peak aging for Alloy-4 can be explained by the coexistence of dislocation-precipitate (D-P) interactions theory [8,13,34,45,51–53]. Therefore, according to the subsequent synopsis, it is assumed that the presence of coherent or semi-coherent precipitates formed at peal aged condition has provided the resistance of dislocation movement and made the slip difficult to proceed, which has led to the increasing the mechanical strength of the Alloy-4. It is widely reported that precipitation of the second

phase during the aging phase can tune mechanical properties by acting as an obstruction to the motion of dislocation by a well-known strengthening mechanism [13,51].

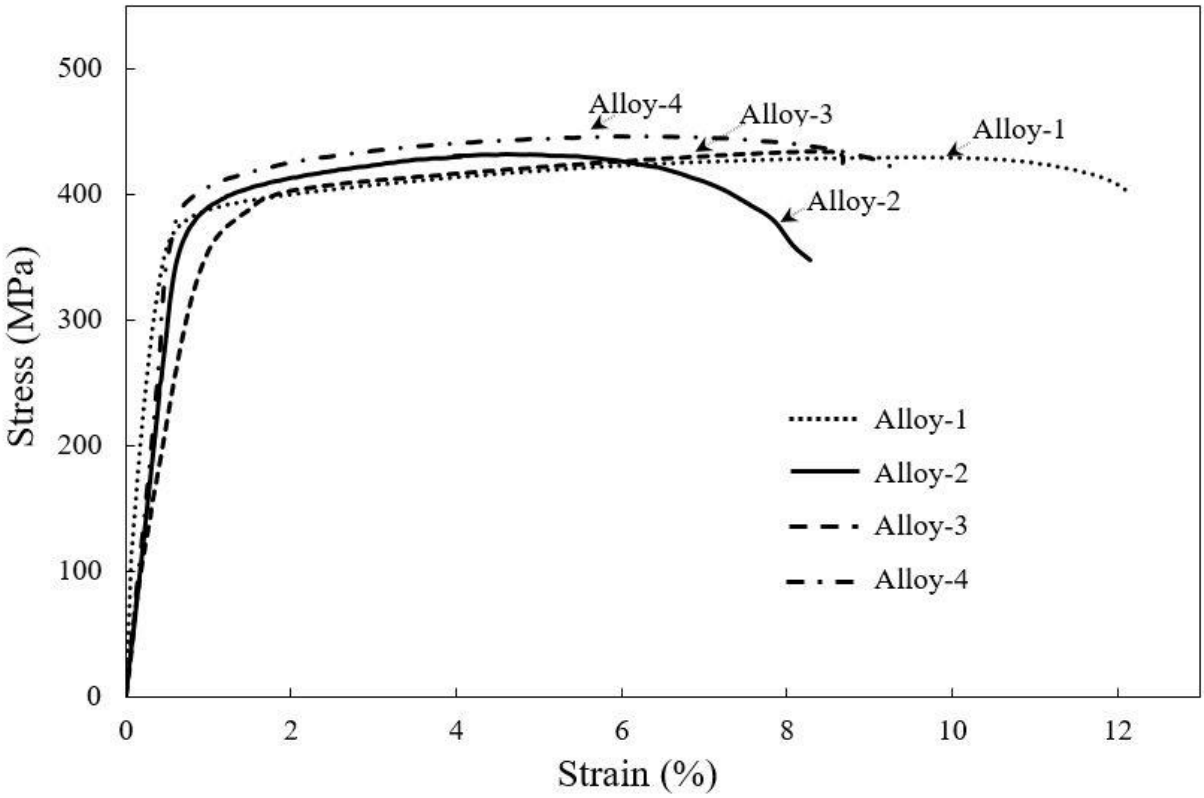

Figure 2. Representative Engineering stress vs. strain curves of the peak aged treated Alloy-1, Alloy-2, Alloy-3 and Alloy-4 specimens.

Table 2. Comparison of hardness values (HV) and ultimate tensile strength (σ_{UTS}) of the presently studies alloys with some traditional Al-based alloys in medical field.

Alloy	Peak Hardness HV	σ_{UTS} MPa.	Ref.
Pure Al	25	90	[8]
7005 T-6 aluminum	197	350	[9]
6061 T-6 aluminum	95	310	[10]
Al-4% Cu-0.5% Mg-0.7% Ag-0.03%Sn(Alloy-4)	142	447	Present study
Al-4% Cu-0.5% Mg-0.3% Ag-0.03%Sn(Alloy-3)	138	434	Present study
Al-4% Cu-0.5% Mg-0.7% Ag-0.01%Sn(Alloy-2)	137	432	Present study
Al-4% Cu-0.5% Mg-0.3% Ag-0.01%Sn(Alloy-1)	136	429	Present study

Thus, according to the present understanding, it can be recapitulated that the phenomenon of increasing strength in our presently studied alloys is strongly dependent on the presence of morphology, size, and volume of microstructural features at the peak aging condition. Therefore, to identify the correlation between the microstructure and mechanical properties at peak-aged conditions, the microstructural observation and phase constituent analysis was carried out for each peak-aged specimen of Alloy-1, Alloy-2, Alloy-3, and Alloy-4, respectively.

3.3. Comparison of the Microstructure of Al-Cu-Mg-Ag-Sn Alloys at Peak-Aged Condition

To elucidate and link the structure-property relationship at the peak aged condition, the optical microscopic (OM) observation was carried out. The optical micrograph reveals the panoramic view of microstructural features such as average grain size (d_{av}) and average precipitate size (μm), which are engendered at the peak aged condition. The average grain size for each Alloy-1, Alloy-2, Alloy-3, and Alloy-4 specimen, respectively, was determined by utilizing the line intercept method. The particle size distribution was also determined by using ImageJ processing software. In general, all the Alloy-1, Alloy-2, Alloy-3, and Alloy-4 specimens revealed equiaxed grains at the peak aged condition, as shown in seen in Figure 3. The black arrows on the OM images, as shown in Figure 3, indicate the fractional number of precipitates within the α-Al (matrix). The average grain sizes for Alloy1, Alloy2, Alloy3, and Alloy4 were determined to be approximately 125 μm, 121 μm, 120 μm, and 106 μm, respectively. One should note that in the OM images of each Alloy-1, Alloy-2, Alloy-3, and Alloy-4 specimens, the multiphase microstructure of secondary phases (intermetallic compound) having different morphology is quite evident. While comparing the precipitate shapes and sizes for each Alloy-1, Alloy-2, Alloy-3, and Alloy-4 specimens, the Alloy-4 specimens reveal a relatively large volume variety of precipitate with different width D, inner precipitate spacing L, and precipitate aspect ratio β morphology and aspect ratio as evidently seen in Figure 3d. Secondly, these results show that the formation of intermetallic phases in our presently studied was mainly dependent on the Sn content and the Ag/Sn ratio. Optical microscopy also revealed micron-scale precipitates on grain as well as sub-micron intragranular precipitates in Alloy-4 specimens. In contrast, with the Alloy-1 specimen, the precipitated phase revealed less volume fraction as seen in Figure 3a. In the next section, the characterization of precipitates was carried out employing energy-dispersive X-ray spectroscopy (EDS). As per our current understanding, the Sn content and Ag/Sn ratio control the dissolution of primary intermetallic precipitates and the formation of precipitates.

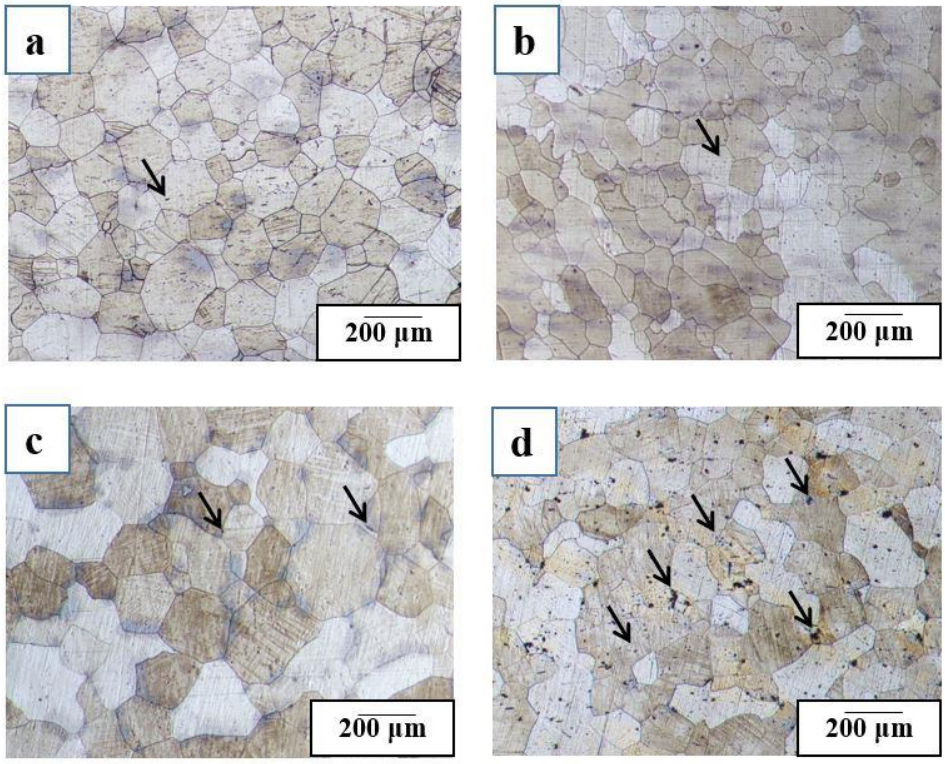

Figure 3. Optical micrographs of the of the peak aged treated: (**a**) Alloy-1; (**b**) Alloy-2; (**c**) Alloy-3; and (**d**) Alloy-4 specimens. The black arrows indicate precipitates with in the α-Al (matrix).

3.4. Identification of Precipitates Using EDS Microanalysis

This section deals with the identification of micron-sized and sub-micron-sized precipitates by energy-dispersive X-ray spectroscopy (EDS). Figure 4, shows the SEM image revealing the precipitate morphology of peak aged treated Alloy-4 specimen. In addition, EDS point analysis measurements in selective areas are also included in tabulated form. Here, white arrows on the SEM image (as seen in Figure 4) indicate the point where EDS analysis was conducted to determine the chemical composition of each region, respectively. The EDS analysis was performed basically for elemental recordings at the locations described above. It can be observed clearly that the white phase (precipitates) is fewer in number, whereas the black phase (precipitates) is larger in number, but its size is in few microns, from the corresponding element weight% content of the most representative phases as summarized in Figure 4. It can be implied that the white precipitate is Cu-rich, and it tends to occur randomly, whereas the black precipitates are Mg-rich and Sn-rich Mg, and their presence are in the form of a network.

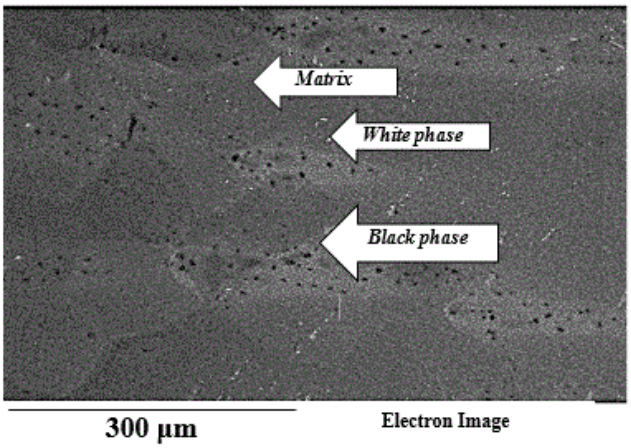

EDX Analysis Matrix		
Element	Weight%	Atomic%
Al	94.19	96.36
Cu	4.36	2.83
Mg	0.49	0.53
Ag	0.71	0.22
Sn	0.03	0.06

EDX Analysis: White phase		
Element	Weight%	Atomic%
Al	76.17	88.27
Cu	23.83	11.73

EDX Analysis: Black phase		
Element	Weight%	Atomic%
Al	99.37	99.20
Mg	0.59	0.77
Sn	0.04	0.08

Figure 4. SEM image showing the characteristic features of the precipitate morphology of peak aged treated Alloy-4. Tables of EDS point analysis measurements in selective areas are also included.

3.5. Comparison of Phase Constitution at Peak Aged Condition

Apart from the EDS analysis, XRD measurements were carried out to complement the description of the several phases as it develops in the presently investigated alloys at the peak aged condition. Figure 5 shows the corresponding XRD profiles of each Alloy-1, Alloy-2, Alloy-3, and Alloy-4 specimens, respectively, at the peak aged condition. From Figure 5, it can be observed that all the specimens exhibited prominent peaks that were indicative of a solid solution of the α-Al phase having a face-centered cubic structure (FCC). For each specimen of Alloy-1, Alloy-2, Alloy-3, and Alloy-4, the intermetallic phases could also be seen from the XRD profiles in addition to the matrix phase (Al) (as shown in Figure 5). These additional peaks could be identified as the Al_2Cu (θ) phase and the Mg_2Sn phase [49]. It is evident that both phases co-existed in Alloy-4 specimens. However, it is

noteworthy that the peak intensity from the Mg_2Sn phase became stronger as the Sn content increased in our designed compositions. It is suggested that the higher contents of Sn might have encouraged the formation of a more complex phase instead of the S-phase. A similar phase has also been previously observed in Al-Cu-Mg-Sn [49]. Overall, EDS and XRD observations were qualitatively correlated and were found to be consistent with each other. However, the EDX and XRD results corroborate the nature of the major phases present in the present study. However, we firmly believe X-ray diffraction patterns cannot record those phases with very small volume ratios or non-homogeneous distribution. Hence TEM is a very important tool, and it would certainly be considered in the further detailed investigation of this alloy and might be reported in our future works.

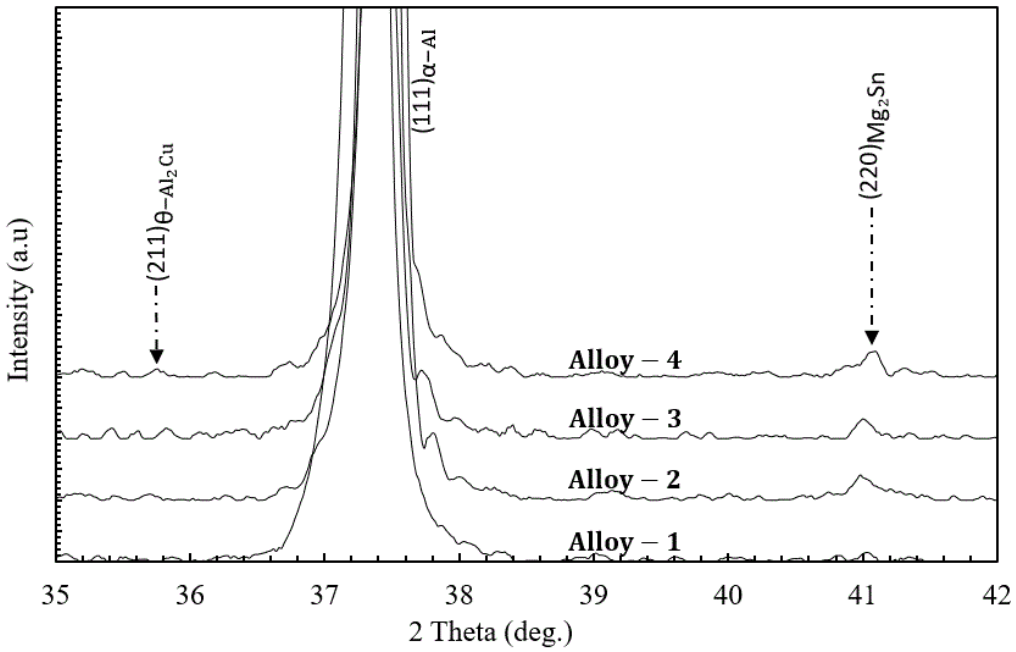

Figure 5. X-ray diffraction (XRD) patterns of the of the peak aged treated Alloy-1, Alloy-2, Alloy-3 and Alloy-4 specimens.

In summary, based on these important comparative microstructural observations, it is plausible that the enhanced mechanical properties, particularly in the case of Alloy-4 specimens, benefited from the existence of conjoint phases in the fcc matrix. Considering these factors, Table 3. enlists the comparative relationship of mechanical properties and the corresponding microstructural features at aged peak conditions for all four alloys, respectively. It is widely known that the mechanical properties of Al-based alloys can be manipulated by controlling the existence and mobility of microscopic crystalline defects [51–57]. In contrast, it is known that the mechanical strengthening phenomenon in Al-based alloys is controlled by immobile crystalline defects, such as precipitates, forest dislocations, and grain boundaries [58,59]. These studies claimed that the precipitation hardening and/or the Orowan bypass stress (τ_{orwan}) collectively depends on the size and shape of precipitates [60,61]. Thus, our preliminary results ubiquitously reflect that the improvement in age-hardening behavior and mechanical strength for the Alloy-4 is mainly due to the coexistence of plate-like Al_2Cu (θ) phase and spherical micron-scaled Mg_2Sn phase, which is resulted by tuning the Sn content (Alloy-4) and tailoring an intermediate Ag/Sn ratio compositional scenarios. Although, in this work, we devote efforts to optimizing the Ag/Sn ratio for improving the mechanical properties of Al-Cu-Mg-*x*Ag-*y*Sn alloy. However, further studies are required to statistically obscure the relationship between precipitation hardening on the dislocation-precipitate bypass mechanism attributed to our developed alloy and will be considered in the future objectives of the research.

Table 3. Comparative relationship of mechanical properties and the corresponding microstructural features at peak aged condition.

Alloy	Avg. Yield Stress σ_{YS} (MPa)	Avg. Tensile—Stress σ_{UTS} (MPa)	Avg. Fracture Stress σ_f (MPa)	Avg. Elongation (%)	Avg. Hardness (HV)	Avg. Grain Size (μm)	Avg. Precipitate Size (μm)	Avg. Peak Aging Time (h)
Alloy-1	355 ± 9	429 ± 11	400 ± 3	12	136	125	5.83	2
Alloy-2	384 ± 7	432 ± 9	348 ± 8	8	137	121	5.17	2
Alloy-3	386 ± 4	434 ± 7	421 ± 5	8	138	120	5.43	2
Alloy-4	387 ± 6	446 ± 8	415 ± 7	9	142	106	4.04	2

4. Conclusions

We devoted our efforts mainly to unveiling a new alloy design approach that incorporation and adjustment of trace elements through Ag/Sn ratio. From our preliminary experimental results, we draw a new alloy design approach for improving the mechanical properties of Al-Cu Mg-based alloys by the incorporation of minor addition of Sn and Ag elements and tailoring the corresponding Ag/Sn ratios. Subsequently, later the focus of this study was on understanding the effect of composition on the mechanical properties of Al-Cu Mg-based alloys. To achieve this objective, the mechanical properties at the peak aged condition were evaluated using tensile testing. We utilize the precipitation-strengthening route to strengthen the fcc-structured Al alloy mainly by obtaining a dual-phase microstructure. Furthermore, the microstructure and phase constituent analysis of the peak aged condition were studied using optical microscopy and XRD. The role of the precipitation strengthening phase was also discussed and compared.

The following conclusions are summarized:

The Ag/Sn ratio has been investigated for the first time in ternary Al-Cu-Mg ternary alloy instead of the conventional Cu/Mg ratio alloy design route.

Among all developed alloys, typically, the Alloy-4, because of the high solute content, exhibited much high hardness and mechanical strength than those of its counterpart. All developed alloys, typically the Alloy-4, because of the high solute content, exhibited much high hardness and mechanical strength than those of its counterpart.

The effect of precipitation hardening effect was more evident in alloys having the highest concentrations of Ag and Sn content simultaneously.

The mechanical properties of our developed alloys were sensitive to composition and resulting strengthening mechanisms.

Optical microscopy and SEM identified the existence of conjoint phases in the fcc matrix.

From XRD profiles, the micron-scaled precipitates were identified as the Mg_2Sn phase.

The Mg_2Sn phase is more denominated in higher content and intermediate Ag/Sn ratio alloy (Alloy-4) when compared to its counterpart.

The Mg_2Sn phase played a key role in increasing the tensile strength by providing the strengthening to the fcc matrix, which is associated with the obstruction to the motion of dislocation of our designed alloys.

The improvement in our presently studied alloying system was very significant when compared to traditional lightweight Al-based alloys already applied in the medical field. For example, Al-4 Cu-0.5 Mg-0.7 Ag-0.03 Sn (wt.%)-T6 (denoted as Alloy-4) exhibited improvement in ultimate tensile strength of more than 300% when compared to pure Al, 44% when compared to 6061 T-6 aluminum and 28% when compared to T-6 aluminum. Thus, it holds great promise to be used as a structural material in the fabrication of exoskeleton frames, prosthetic, and wheelchair components.

Author Contributions: Conceptualization, M.F.I. and F.H.H.; methodology, F.H.H.; software, F.H.H.; validation, M.F.I. and F.H.H.; formal analysis, M.F.I.; investigation, M.F.I. and F.H.H.; resources, M.F.I.; data curation, F.H.H.; writing—original draft preparation, M.F.I.; writing—review and editing, F.H.H.; visualization, M.F.I. and F.H.H.; supervision, M.F.I.; project administration, M.F.I.; funding acquisition, M.F.I. All authors have read and agreed to the published version of the manuscript.

Funding: I am grateful and extend appreciation to the King Salman center For Disability Research for funding this work through Research Group no KSRG-2022-033.

Institutional Review Board Statement: Not applicable.

Informed Consent Statement: Not applicable.

Data Availability Statement: The datasets generated during and/or analyzed during the current study are available from the corresponding author upon reasonable request.

Acknowledgments: The authors extend their main appreciation to the King Salman center For Disability Research for funding this work through Research Group no KSRG-2022-033. We would also like to thank the College of Engineering Research center and lab facilities at King Saud University in Riyadh, Saudi Arabia.

Conflicts of Interest: The authors declare no conflict of interest.

References

1. Bronzino, J.D.; Peterson, D.R. *Biomedical Engineering Fundamentals*; CRC Press: Boca Raton, FL, USA, 2014.
2. Cooper, R.A.; Ohnabe, H.; Hobson, D.A. *An Introduction to Rehabilitation Engineering*; CRC Press: Boca Raton, FL, USA, 2006.
3. Thurston, A.J. Paré and prosthetics: The early history of artificial limbs. *ANZ J. Surg.* **2007**, *77*, 1114–1119. [CrossRef] [PubMed]
4. Cooper, R.A.; Cooper, R. Rehabilitation Engineering: A perspective on the past 40-years and thoughts for the future. *Med. Eng. Phy.* **2019**, *72*, 3–12. [CrossRef] [PubMed]
5. ASM Handbook Committee. *Properties and Selection: Nonferrous Alloys and Special-Purpose Materials*; ASM International: Russell Township, OH, USA, 1990.
6. Spada, A.T. In Search of Lightweight Components: Automotive Cast Aluminum Conversion. *Eng. Cast. Solut.* **2002**, *4*, 28–31.
7. ASM International. *Properties and Selection of Aluminum Alloys*; ASM International: Russell Township, OH, USA, 2019.
8. Davis, J.R. *Aluminum and Aluminum Alloys. Alloying: Understanding the Basics*; ASM International: Russell Township, OH, USA, 1993; pp. 351–416.
9. Liu, H.-Y.; Pearlman, J.; Cooper, R.; Hong, E.-K.; Wang, H.; Salatin, B.; Cooper, R.A. Evaluation of aluminum ultralight rigid wheelchairs versus other ultralight wheelchairs using ANSI/RESNA standards. *J. Rehabil. Res. Dev.* **2010**, *47*, 441–455. [CrossRef] [PubMed]
10. Gebrosky, B.; Pearlman, J.; Cooper, R. Comparison of High-Strength Aluminum Ultralight Wheelchairs Using ANSI/RESNA Testing Standards. *Top Spinal Cord Inj. Rehabil.* **2018**, *24*, 63–77. [CrossRef] [PubMed]
11. Hatch, J.E. Effects of alloying elements and impurities on properties. In *Aluminum: Properties and Physical Metallurgy*; ASM International: Russell Township, OH, USA, 1983; pp. 200–241.
12. Erickson, R.B.; Murtha, S.J. Highly Formable Aluminum Alloy Rolled Sheet. U.S. Patent 5,582,660, 10 December 1996.
13. Guinier, A. Structure of age-hardened aluminium-copper alloys. *Nature* **1938**, *142*, 569. [CrossRef]
14. Totten, G.E.; MacKenzie, D.S. (Eds.) *Handbook of Aluminum, Vol. 1: Physical Metallurgy and Process*; Marcel Dekker Inc.: New York, NY, USA, 2003; pp. 114–168.
15. Kanno, M.; Suzuki, H.; Kanoh, O. The precipitation of θ′ phase in an Al-4%Cu-0.06%In alloy. *J. Jpn. Inst. Metals* **1980**, *44*, 7. [CrossRef]
16. Liu, L.; Chen, J.H.; Wang, S.B.; Liu, C.H.; Yang, S.S.; Wu, C.L. The effect of Si on precipitation in Al–Cu–Mg alloy with a high Cu/Mg ratio. *Mater. Sci. Eng. A* **2014**, *606*, 187–195. [CrossRef]
17. Wang, S.C.; Starink, M.J.; Gao, N. Overview of recent work on precipitation in Al-Cu-Mg alloys. In *Materials Science Forum*; Trans Tech Publications Ltd.: Stafa-Zurich, Switzerland, 2007.
18. Wang, S.C.; Starink, M.J. Two types of S phase precipitates in Al-Cu-Mg alloys. *Acta Mater.* **2007**, *55*, 933–941. [CrossRef]
19. Starink, M.J.; Yan, J.L. Precipitation hardening in Al-Cu-Mg alloys: Analysis of precipitates, modelling of kinetics, strength predictions. In *Materials Science Forum*; Trans Tech Publications Ltd.: Stafa-Zurich, Switzerland, 2006.
20. Brook, G.B. *Precipitation in Metals*; Special Rept. No. 3; Fulmer Research Institute: Stoke Poges, UK, 1963.
21. Liu, Z.R.; Chen, J.H.; Wang, S.B.; Yuan, D.W.; Yin, M.J.; Wu, C.L. The structure and the properties of S-phase in AlCuMg alloys. *Acta Mater.* **2011**, *59*, 7396–7405. [CrossRef]
22. Ijaz, M.F.; Soliman, M.S.; Alasmari, A.S.; Abbas, A.T.; Hashmi, F.H. Comparison of Mechanical and Microstructural Properties of as-Cast Al-Cu-Mg-Ag Alloys: Room Temperature vs. High Temperature. *Crystals* **2021**, *11*, 1330. [CrossRef]
23. Alshammari, T.T.; Alharbi, H.F.; Soliman, M.S.; Ijaz, M.F. Effects of Mg Content on the Microstructural and Mechanical Properties of Al-4Cu-xMg-0.3Ag Alloys. *Crystals* **2020**, *10*, 895. [CrossRef]

24. Abdo, H.S.; Seikh, A.H.; Muhammad, J.A.; Soliman, M.S. Alloying Elements Effects on Electrical Conductivity and Mechanical Properties of Newly Fabricated Al Based Alloys Produced by Conventional Casting Process. *Materials* **2021**, *14*, 3971. [CrossRef] [PubMed]
25. Wang, J.; Liu, Z.; Bai, S.; Cao, J.; Zhao, J.; Luo, L.; Li, J. Microstructure evolution and mechanical properties of the electron-beam welded joints of cast Al-Cu-Mg-Ag alloy. *Mater. Sci. Eng. A* **2021**, *801*, 140363. [CrossRef]
26. Tiryakioglu, M.; Campbell, J. Ductility, structural quality, and fracture toughnessof Al-Cu-Mg-Ag (A201) alloy castings. *Mater. Sci. Technol.* **2009**, *25*, 784–789. [CrossRef]
27. Zamani, M.; Toschi, S.; Morri, A.; Ceschini, L.; Seifeddine, S. Optimisation of heat treatment of Al-Cu-(Mg-Ag) cast alloys. *J. Therm. Anal. Calorim.* **2020**, *139*, 3427–3440. [CrossRef]
28. Li, J.F.; Ziqiao, Z.; Na, J.; Chengyu, T. Localized corrosion mechanism of 2×××-series Al alloy containing S(Al2CuMg) and θ (Al2Cu) precipitates in 4.0% NaCl solution at pH 6.1. *Mater. Chem. Phys.* **2005**, *91*, 325–329. [CrossRef]
29. AGupta, K.; Gaunt, P.; Chaturvedi, M.C. The crystallography and morphology of the S′-phase precipitate in an Al(CuMg) alloy. *Philos. Mag. A* **1987**, *55*, 375–387.
30. So, H.; Won, S.; Oh, J.P.S.J.; Kang, L.; Kim, K. Mechanical properties and microstructural evolution in Al–Cu–Mg–Ag alloy with a CuxMgx/10 content. *Mater. Sci. Eng. A* **2021**, *824*, 141573. [CrossRef]
31. Chester, R.J.; Polmear, I.J. *The Metallurgy of Light Alloys*; Institution of Metallurgists: London, UK, 1983.
32. Taylor, J.A.; Parker, B.A.; Polmear, I.J. Precipitation in AI-Cu-Mg-Ag casting alloy. *Met. Sci.* **1978**, *12*, 478–482. [CrossRef]
33. Zheng, Y.; Xiao, W.L.; Ge, S.J.; Zhao, W.T.; Hanada, S.; Ma, C.L. Effects of Cu content and Cu/Mg ratio on the microstructure and mechanical properties of Al-Si-Cu-Mg alloys. *J. Alloys Compd.* **2015**, *649*, 291–296. [CrossRef]
34. Ringer, S.P.; Yeung, W.; Muddle, B.C.; Polmear, I.J. Precipitate stability in Al-Cu-MgAg alloys aged at high temperatures. *Acta Metall. Mater.* **1994**, *42*, 1715–1725. [CrossRef]
35. Silcock, J.M.; Heal, T.J.; Hardy, H.K. The structural aging characteristics of ternary aluminum-copper alloys with cadmium, indium, or tin. *J. Inst. Met.* **1955**, *84*, 13.
36. Ringer, S.P.; Hono, K.; Sakurai, T. The effect of trace additions of Sn on precipitation in Al-Cu alloys—An atom probe field ion microscopy study Metall. *Mater. Trans. A* **1995**, *26A*, 11. [CrossRef]
37. Ringer, S.P.; Hono, K.; Sakurai, T. Nucleation and growth of θ′ precipitation in Sn-modified Al-Cu alloys: APFIM/TEM observations. *Appl. Surf. Sci.* **1995**, *87/88*, 223. [CrossRef]
38. Bourgeois, L.; Nie, J.F.; Muddle, B.C. Assisted nucleation of θ′ phase in Al–Cu–Sn: The modified crystallography of tin precipitates. *Philos. Mag.* **2005**, *85*, 3487–3509. [CrossRef]
39. Bourgeois, L.; Dwyer, C.; Weyland, M.; Nie, J.F.; Muddle, B.C. The magic thicknesses of θ′ precipitates in Sn micro-alloyed Al–Cu. *Acta Mater.* **2012**, *60*, 633–644. [CrossRef]
40. Bourgeois, L.; Nie, J.F.; Muddle, B.C. On the role of tin in promoting nucleation of the θ′ phase in Al-Cu-Sn. *Mater. Sci. Forum* **2002**, *396–402*, 789–794.
41. Honma, T.; Saxey, D.W.; Ringer, S.P. Effect of trace addition of Sn in Al-Cu alloy. *Mater. Sci. Forum* **2006**, *519–521*, 203–208.
42. Homma, T.; Moody, M.P.; Saxey, D.W.; Ringer, S.P. Effect of Sn addition in precipitation stage in Al-Cu alloys: A correlative transmission electron microscopy and atom probe tomography study Metall. *Mater. Trans. A* **2012**, *43*, 2192–2202. [CrossRef]
43. Shu, J.; Chen, Z.G.; Zhang, J.S. Effects of microalloying with Sn on the precipitation process of Al-3.5Cu-0.4Mg (wt%) alloy. In Proceedings of the 13th International Conference on Aluminum Alloys, Pittsburgh, PA, USA, 3–7 June 2012; John Wiley & Sons: Hoboken, NJ, USA, 2012.
44. Banerjee, S.; Robi, P.S.; Srinivasan, A. Calorimetric study of precipitation kinetics of Al-Cu-Mg and Al-Cu-Mg-0.06 wt.% Sn alloys. *Met. Mater. Int.* **2010**, *16*, 523–531. [CrossRef]
45. Banerjee, S.; Robi, P.S.; Srinivasan, A.; Lakavath, P.K. Effect of trace additions of Sn on microstructure and mechanical properties of Al–Cu–Mg alloys. *Mater. Des.* **2010**, *31*, 4007–4015. [CrossRef]
46. Banerjee, S.; Robi, P.S.; Srinivasan, A.; Kumar, L.P. High-temperature deformation behavior of Al–Cu–Mg alloys micro-alloyed with Sn. *Mater. Sci. Eng. A* **2010**, *527*, 2498–2503. [CrossRef]
47. Poon, I.; Marceau, R.K.W.; Xia, J.; Liao, X.Z.; Ringer, S.P. Precipitation processes in Al-Cu-Mg-Sn and Al-Cu-Mg-Sn-Ag. *Mater. Des.* **2016**, *96*, 385–391. [CrossRef]
48. Wolverton, C. Solute–vacancy binding in aluminum. *Acta Mater.* **2007**, *55*, 5867–5872. [CrossRef]
49. Dai, S.; Bian, Z.; Wu, W.; Tao, J.; Cai, L.; Wang, M.; Xia, C.; Wang, H. The role of Sn element on the deformation mechanism and precipitation behavior of the Al–Cu–Mg alloy. *Mater. Sci. Eng. A* **2020**, *792*, 139838. [CrossRef]
50. Kittel, C. *Introduction to Solid State Physics*, 7th ed.; John Wiley: New York, NY, USA, 1996; p. 78.
51. Embury, J.; Lloyd, D.; Ramachandran, R. 22—Strengthening mechanisms in aluminum alloys. *Treatise Mater. Sci. Technol.* **1989**, *31*, 579–601.
52. Polmear, I.J. Aluminium Alloys-A Century of Age hardening. *Mater. Sci. Forum* **2004**, *28*, 1–14.
53. Hirth, J.P.; Lothe, J. *Theory of Dislocations*, 2nd ed.; Wiley: New York, NY, USA, 1982.
54. Foreman, A.J.E.; Makin, M.J. Dislocation movement through random arrays of obstacles. *Philos. Mag.* **1966**, *14*, 911–924. [CrossRef]
55. Gladman, T. Precipitation hardening in metals. *Mater. Sci. Technol.* **1999**, *15*, 30–36. [CrossRef]
56. Ashby, M.F. Work hardening of dispersion-hardened crystals. *Philos. Mag. A J. Theor. Exp. Appl. Phys.* **1966**, *14*, 1157–1178. [CrossRef]

57. Bacon, D.J.; Osetsky, Y.N.; Rodney, D. *Dislocations in Solids*; Elsevier: North-Holland, The Netherlands, 2009; Volume 15.
58. Dérès, J.; Proville, L.; Marinica, M.C. Dislocation depinning fromnano-sized irradiation defects in a bcc iron model. *Acta Mater.* **2015**, *99*, 99–105. [CrossRef]
59. Queyreau, S.; Monnet, G.; Devincre, B. Orowan strengtheningand forest hardening superposition examined by dislocation dynamics simulations. *Acta Mater.* **2010**, *58*, 5586–5595. [CrossRef]
60. Nembach, E. *Particle Strengthening of Metals and Alloys*; John Wiley & Sons: Hoboken, NJ, USA, 1997.
61. Szajewski, B.; Crone, J.C. Analytic model for the Orowan dislocation-precipitate bypass mechanism. *Materialia* **2020**, *11*, 100671. [CrossRef]

crystals

an Open Access Journal by MDPI

CITESCORE 3.2

IMPACT FACTOR 2.670

CERTIFICATE OF SERVICE

AS

Guest Editor of Special Issue

"Recent Advances in Light Alloys"

Dr. Muhammad Farzik Ijaz

Mechanical Engineering Department, College of Engineering, King Saud University, P.O. Box 800, Riyadh 11421, Saudi Arabia

MDPI Academic Open Access Publishing since 1996

Basel, November 2022

Dr. Shu-Kun Lin

Publisher & President